ACS APPLIED MATERIALS & INTERFACES

Research Article

www.acsami.org

Encapsulation of Perovskite Nanocrystals into Macroscale Polymer Matrices: Enhanced Stability and Polarization

Shilpa N. Raja,[†,∥] Yehonadav Bekenstein,[‡,∥,⊥] Matthew A. Koc,[‡,∥] Stefan Fischer,[‡,∥] Dandan Zhang,[‡,∥] Liwei Lin,[§] Robert O. Ritchie,[†,§,∥] Peidong Yang,[†,‡,∥,⊥] and A. Paul Alivisatos*[,†,‡,∥,⊥]

[†]Department of Materials Science and Engineering, [‡]Department of Chemistry, and [§]Department of Mechanical Engineering, University of California, Berkeley, California 94720, United States

[∥]Materials Sciences Division, Lawrence Berkeley National Laboratory, Berkeley, California 94720, United States

[⊥]Kavli Energy NanoScience Institute, Berkeley, California 94720, United States

Supporting Information

ABSTRACT: Lead halide perovskites hold promise for photonic devices, due to their superior optoelectronic properties. However, their use is limited by poor stability and toxicity. We demonstrate enhanced water and light stability of high-surface-area colloidal perovskite nanocrystals by encapsulation of colloidal $CsPbBr_3$ quantum dots into matched hydrophobic macroscale polymeric matrices. This is achieved by mixing the quantum dots with presynthesized high-molecular-weight polymers. We monitor the photoluminescence quantum yield of the perovskite−polymer nanocomposite films under water-soaking for the first time, finding no change even after >4 months of continuous immersion in water. Furthermore, photostability is greatly enhanced in the macroscale polymer-encapsulated nanocrystal perovskites, which sustain $>10^{10}$ absorption events per quantum dot prior to photodegradation, a significant threshold for potential device use. Control of the quantum dot shape in these thin-film polymer composite enables color tunability via strong quantum-confinement in nanoplates and significant room temperature polarized emission from perovskite nanowires. Not only does the high-molecular-weight polymer protect the perovskites from the environment but also no escaped lead was detected in water that was in contact with the encapsulated perovskites for months. Our ligand-passivated perovskite-macroscale polymer composites provide a robust platform for diverse photonic applications.

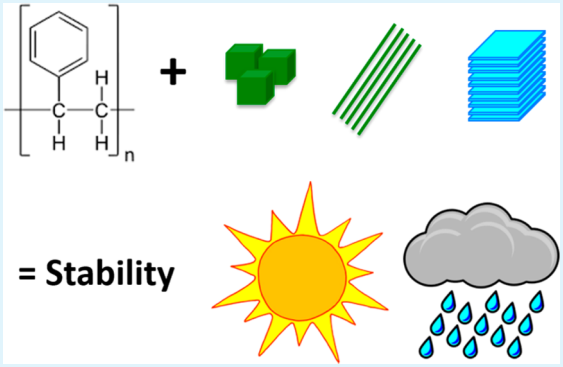

KEYWORDS: *perovskite quantum dot nanocrystals, hydrophobic polymer, nanocomposite polarization, light and water stability, photon budget, nanowires and nanoplates*

INTRODUCTION

In recent years, metal halide perovskites (e.g., methylammonium lead bromide ($CH_3NH_3PbBr_3$) and cesium lead bromide ($CsPbBr_3$)) have been in the spotlight as highly promising optical device materials.[1−3] These materials display high quantum yields and long lifetimes which result in highly efficient backlight displays[4] and photodetectors.[5,6] However, their poor stability, due to their ionic nature and low melting temperatures, and environmental impact, from lead toxicity,[7] have raised major concerns over their large-scale applicability.[8] Recently, colloidal perovskite quantum dots (QDs) were synthesized with high photoluminescence quantum yield.[9−11] Such perovskite nanocrystals display narrow spectral line widths,[1] low lasing thresholds,[12] colloidal dispersibility,[9] and a composition- and size-tunable band gap. Colloidal perovskites differ from other nanostructured perovskites by their native alkyl-chain surface passivation.[9] The hydrophobicity of these ligands offers increased tolerance to humidity in comparison to that of polycrystalline thin film methylammonium lead halide devices.[1,13,14] Recent studies have further shown that irradiating perovskite QD films with X-rays cross-links ligands and provides some stability to UV light and moisture,[15] although the ligand shell alone cannot prevent degradation of the nanocrystals upon long-term, direct contact with water.[16−18] Polymeric encapsulation, i.e., the incorporation of semiconductors into macroscale, presynthesized, high-molecular-weight (≥50 kDa) polymer matrices to prepare thin films, is a common method for protection of semiconductor devices from the environment.[19] This method does not employ polymeric capping ligands and is in contrast to studies that seek to protect quantum dots from the environment by coating them with small oligomeric ligands.[20,21] With lead-halide perovskites, to date encapsulation into macroscale polymeric matrices has generally seen limited or mixed success for water stability due

Received: July 29, 2016
Accepted: December 6, 2016
Published: December 6, 2016

DOI: 10.1021/acsami.6b09443
ACS Appl. Mater. Interfaces 2016, 8, 35523−35533

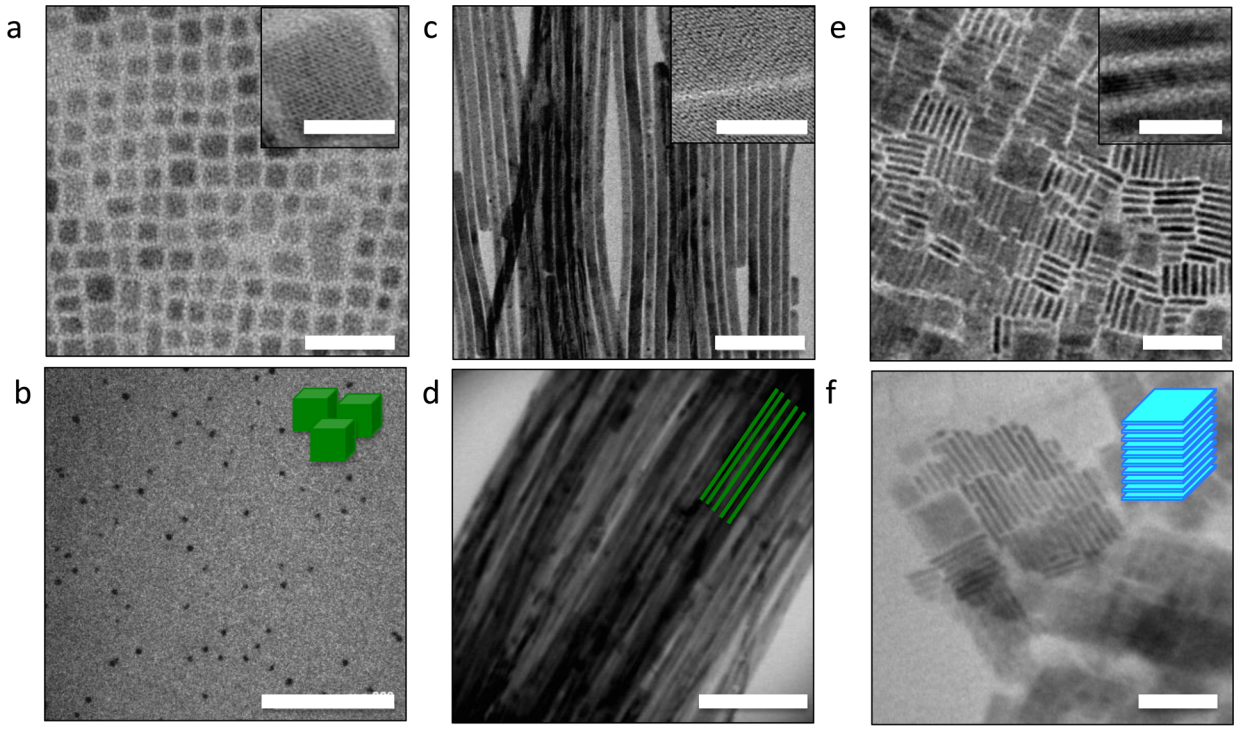

Figure 1. (a) TEM micrograph of zero-dimensional $CsPbBr_3$ nanocubes. The inset high-resolution image illustrates the crystallinity of individual nanocubes. Scale bar is 30 and 8 nm for inset. (b) TEM micrograph of a ∼ 200 nm thick composite film, illustrating that nanocubes are also singly dispersed after insertion into SEBS polymer; the size of nanocubes remains the same ∼8 ± 1 nm within error before and after polymer encapsulation. Scale bar is 200 nm. (c) One-dimensional single nanowires segregate to form bundles and are challenging to separate. Scale bars are 100 and 10 nm for inset. (d) After insertion into a polymer the bundles retain their overall size and structure. Scale bar is 200 nm. (e) When dried, two-dimensional perovskite nanoplates tend to stack forming columnar phases. Scale bars are 50 and 10 nm for inset. (f) TEM micrograph of perovskite nanoplates after insertion into a polymer, individual nanoplates are seen in a stacked array. Scale bar is 50 nm. (b, d, f) Insets are cartoons of the three different shapes in this work.

to poor interfacial contact between the perovskite and polymer, e.g., thin film devices coated with a polymeric layer still degrade within minutes upon immersion in water.[17,18,22] Colloidal QDs, with their high surface area, demonstrate effective polymeric encapsulation.[23] By matching QD surface chemistry and polymeric properties, highly dispersed composites can be made with increased bulk polymer−ligand adhesion.[23] In recent work, Protesescu et al.[9] initially demonstrated the incorporation of perovskite QDs into the hydrophilic poly(methyl methacrylate) but did not perform measurements of stability or dispersion. Subsequent work by Pathak et al. demonstrates the potential for white-light LEDs by embedding perovskite QDs into polymers.[24] Further work by Wang et al. demonstrated improved thermal stability and 30 min of stability in boiling water via polymer encapsulation,[25] and Rogach et al. demonstrated bright emission qualitatively, i.e., digital images, after 10 weeks of soaking polymer-coated QDs in water but did not assess the quantum yield or spectral features of the QDs before and after water soaking.[21] While these works were substantial advancements, spectral shifts and reductions in quantum yield can substantially affect their use in optical device applications. Thus, there is a need for more quantitative experimental follow-up investigations, i.e., monitoring of spectral peak positions and quantum yield, of the susceptibility of perovskite QD−polymer composites to light and water. Of particular interest is the study of macroscale polymeric encapsulation, due to its inexpensive and facile application as compared to time-consuming ligand-exchange protocols which are still very limited for perovskite QDs.[26] By contrast, bulk polymers are inexpensive, and encapsulation can readily be achieved. As a result, stabilizing quantum dots with this method is potentially much more commercially viable than other methods employing oligomeric capping ligands.

Here we incorporate hydrophobic $CsPbBr_3$ QDs into water-repelling hydrophobic bulk polymers and demonstrate dramatically enhanced light and water stabilities, including retention of quantum yield for several months of water-soaking and reduced lead toxicity. Colloidal synthesis can enable the control of the shape and structure of QDs, significantly affecting their optoelectronic properties. We utilize these previously established techniques and examine the added functionalities associated with the different monocrystalline shapes embedded in the polymeric matrices, specifically polarization in micrometer-long nanowires,[11] and color tuning in strongly quantum-confined nanoplates.[10] We explore the generality of our results by expanding our study to three different hydrophobic macroscopic polymer matrices.

The novelty of this strategy is twofold. First, the perovskite QDs are extremely sensitive to the hydrophobicity of the chosen polymeric matrix. Their sensitivity arises due to their ionic-crystal nature and dynamic ligand surface coverage. As a result solvents with polarity index greater 4.4, e.g ethyl-acetate, will degrade the particles. Therefore, when choosing the polymeric matrix for encapsulation, extra care should be taken to choose a hydrophobic enough polymer and a compatible solvent. Second, the unusual dynamic nature of the surface ligands may result in the loss of ligands in the encapsulation process which greatly affects the QDs electronic properties and

DOI: 10.1021/acsami.6b09443
ACS Appl. Mater. Interfaces 2016, 8, 35523−35533

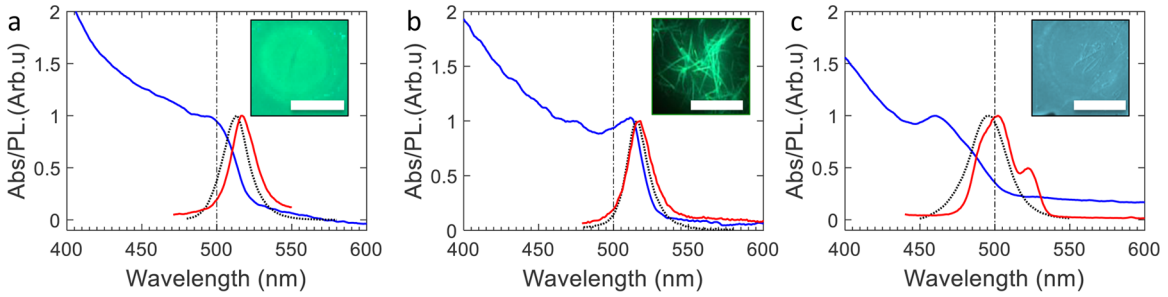

Figure 2. (a) Normalized absorption (blue) and emission spectra of QD−polymer composites before (gray) and after (red) spin-casting polystyrene-composites on glass substrates. Emission from dry nanocube−polymer composites demonstrate a red-shifting of 2 ± 1 nm. (b) The emission peak fwhm of spun-cast nanowire-composites shows 2 ± 1 nm broadening and no peak shift. (c) Nanoplate composites demonstrate a strongly quantum-confined, blue-shifted emission (λ_{max} = 494 nm) which red-shifts by 6 ± 1 nm upon drying, resulting in composites that emit bluer light (λ_{max} = 502 nm) compared to nanocubes (λ_{max} = 517 nm). Dashed line is an eye guide. Spun-cast glass with nanocube−polymer and nanoplate−polymer composites under UV illumination (a and c) insets respectively; scale bar is 5 mm). (b, inset). Microscope image of spun-cast nanowire−polymer composites (excited with 488 nm laser light) showing random orientation of wire-bundles. Scale bar is 30 μm.

photoluminescence quantum yield (PLQY). In this work, we use polymers like poly(styrene-ethylene-butylene-styrene) (SEBS) which contain alkyl chain ligands of very similar composition to the native alkyl chain ligands (oleylamine and oleic acid) on the quantum dot surface. This matching creates a better QD−polymer interface than that with less hydrophobic polymers. The matched interface minimizes ligand loss in the encapsulation process and minimizes water and oxygen molecules diffusion to the QD surface. This is likely the reason for the greater stability seen in our work over previous works.

We build on the above-mentioned previous works by assessing spectral shifts and quantum yield upon exposure to light and water, finding that the perovskite polymer films retain stable quantum yield when soaking in water for periods of more than 4 months. We associate this with the dense alkyl chain coverage of the as-synthesized QDs,[27] which unlike most previous works, matches the hydrophobic nature of the encapsulating polymers.[28] Moreover, in the polymer, the perovskite QDs are far more resistant to photodegradation under continuous-wave visible laser illumination, surviving in some cases $>10^{10}$ absorption events per QD prior to photodegradation, a significant threshold for any excited fluorophore.[29,30] Recent studies have shown a factor of 3 improved stability to light in color-conversion light-emitting diodes by incorporating short-chain polymers or oligomers into the QD ligand shell during the synthetic process.[31] We expand upon and complement these works by studying the light stability in bulk polymers (no ligand exchange employed) under a variety of light fluxes, finding orders of magnitude higher light stability upon encapsulation. While the polymers in this work are insulating, our results could readily be extended to semiconducting polymers which are matched with the tunable ligand shell of the perovskite QDs for light-emitting devices. This study demonstrates record enhanced photostability,[29,30] photoluminescence polarization,[32,33] and quantum yield retention upon water expsoure[17] for encapsulated lead-halide perovskites.[8] Furthermore, we did not detect any increase in lead content in the water that was in contact with the composites for months. Our results demonstrate the significant potential of polymer encapsulation into macroscale polymeric matrices for perovskite QDs in real-world situations where stability and lead toxicity are major concerns.[8,18]

UNIQUE FUNCTIONALITIES IN PEROVSKITE−POLYMER COMPOSITES

Composites were formed by mixing solutions of QDs and hydrophobic−polymers in toluene (see Methods). Specifically, we studied polystyrene (PS) which was spun-cast into thin films and its derivative, SEBS (poly(styrene-ethylene-butylene-styrene)), which is highly ductile and can be drop-cast into thick samples that are optically clear. SEBS is a widely used low-cost structural triblock copolymer which is a thermoplastic elastomer;[28,34] it combines high formability and recyclability with high toughness. We also studied composites of poly(lauryl methacrylate) (PLMA) which is a highly viscous liquid at room temperature.[35]

We use perovskite QD colloidal synthesis techniques to change the dimensionality and shape of the QDs, thus varying the macroscopic physical properties of the composites. Specifically, we synthesized $CsPbBr_3$ zero-dimensional cubes, one-dimensional wires, and two-dimensional plates.[9−11] The resulting nanocubes were 8 ± 1 nm in size. Plates were 20−30 nm in the lateral dimension and 2.4 and 3 nm in thickness, which correspond to 4 and 5 perovskite unit cells. Wires were 10 nm thick and several micrometers long. Figure 1a shows a transmission electron micrograph (TEM) and high-resolution TEM (HRTEM) (inset) of the nanocubes cast from hexane. The nanocube−polymer solutions were mixed at appropriate concentrations and were spun-cast or drop-cast onto glass substrates and dried overnight. The resulting films with an optical density of 0.075−1 and varying thicknesses, 1.5−3 μm (PS) and 150 μm (SEBS), were then characterized and their stability tested. Figure 1b shows a TEM micrograph of such a composite film with a thickness <200 nm. At low concentrations (OD < 0.2), nanoparticles are singly dispersed and distributed evenly throughout the polymer, while assemblies are formed at higher concentrations.[36] In the polymer, as the three-dimensional cubes take random orientations; it is challenging to resolve the cubic faceting in a two-dimensionally projected TEM image (Figure S1). Statistical analysis of TEM micrographs shows retention of size before and after embedding nanocubes into SEBS polymer (see Methods).

Figure 1c,e shows TEM and HRTEM (inset) images of $CsPbBr_3$ nanowires and nanoplates cast from hexane and those embedded in SEBS (Figure 1d,f). The nanoplates self-assemble into stacked arrays forming columnar phases clearly visible in

DOI: 10.1021/acsami.6b09443
ACS Appl. Mater. Interfaces 2016, 8, 35523−35533

the micrographs. The micrometer-long nanowires have a tendency to form wire bundles along the long axis, probably due to partial loss of surface passivation during their long synthesis process.[11,37]

We studied the optical properties of the nanocomposites. We make use of the bright PL emission of the perovskite crystallites to learn about the microscopic environment they are experiencing when integrated into the polymeric matrices. We compare the three different shapes when embedded into bulk polystyrene. Figure 2 depicts the absorption and emission spectra of the composite solution and also emission of resulting dry composite films for the three QD geometries. In general, the optical properties of the composite solutions are similar to those of the as-synthesized QDs (Figure S1). Forming a dried film from the composites tends to red-shift the emission peak by (a) 2 ± 1 nm for the nanocubes and more significantly by (c) 6 ± 0.5 nm for the nanoplates. Almost no shifts were measured for the bundle-forming nanowires. We assign these optical characteristics to the structural integrity of the quantum confined crystals. The cubes are well dispersed both in hexane and the polymer and experience little red-shifting, probably due to residual aggregation.

The plates exhibit a much more significant change. First, the extent of the shift and overall broadening of the central peak is larger (shift of 6 ± 0.5 nm compared to 2 ± 1 in cubes), and in addition, the appearance of a red-shifted peak observed at 525 ± 1 nm is assigned to aggregation and total loss of confinement. Both of these observations suggest that the nanoplates which are strongly quantum-confined in the *z*-dimension are more sensitive to structural changes which occur during polymeric encapsulation.

Nanowires displayed the most tolerance to polymeric encapsulation due to their intrinsic tendency to from bundles after synthesis even when in hexane. Due to their large surface areas, they already display aggregated PL emission even in hexane; therefore, their spectra is unchanged when put into the polymer matrices.

Bundles of nanowires in drop-cast polymeric films are randomly oriented, as illustrated in the optical microscope image (Figure 2b, inset). By mechanically stretching the polymeric matrix to form long, thin fibers, internal shear forces align the nanowire bundles along the pulling direction. To demonstrate this, we use the highly stretchable nanowire–PLMA composites. In Figure 3a, this macroscopic alignment can be observed when imaged by fluorescent microscopy and a confocal microscope. Using linear polarizers, the emission intensity from a fiber containing many aligned bundles as a function of the polarizer angle was measured. The degree of polarization was determined as the ratio $P = (I_{\parallel} - I_{\perp})/(I_{\parallel} + I_{\perp})$, where $I_{\parallel}$ and $I_{\perp}$ are, respectively, the intensities of the polarized emission in the directions parallel and perpendicular to the direction of the composite fiber. Figure 3b shows a polarization ratio of 0.44 ± 0.05 in the aligned nanowire–polymer composite emission, as compared to 0.08 ± 0.01 in the case of nanocube–polymer composites, where the two samples are prepared and measured under the same conditions. Polarized emission in 1D semiconducting InP wires and CdSe rods is well-documented with high polarization ratios of 0.96 and 0.86, respectively.[38,39] In $CsPbBr_3$ very small polarization ratios were initially reported in nanocrystalline samples at liquid helium temperatures and attributed to anisotropy in quantum confinement effects due to crystal shape.[32] Recently, it has been shown that $CsPbI_3$ colloidal nanocubes also emit

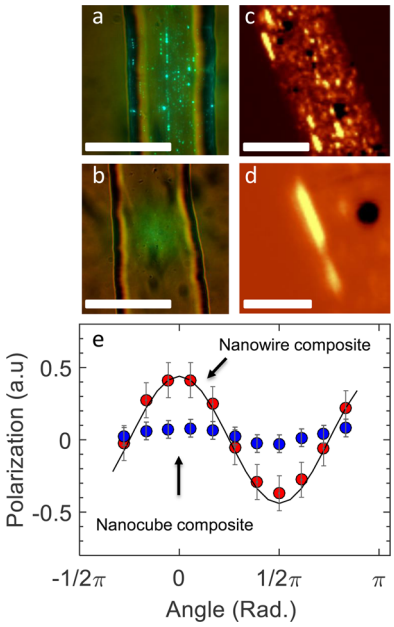

Figure 3. Polarized emission from aligned perovskite nanowires. (a) Optical microscope image of a mechanically drawn nanowire–polymer (PLMA) composite fiber. Shear forces align the high aspect ratio (>100) nanowire bundles parallel to the long axis of the polymer composite fiber. The nanowires are excited with 456 nm laser light and emit green 517 nm light. (b) Nanocube–polymer composite fibers fabricated with the same conditions do not show similar alignment. Scale bar, 20 μm. (c) Confocal microscope image of emitted light (band-pass filter 514 ± 10 nm) depicting the alignment of bundles inside the fiber and a close-up depicting (d) two such aligned bundles. (e) Calculated polarization ($P = \frac{I_{\parallel} - I_{\perp}}{I_{\parallel} + I_{\perp}}$) as a function of polarized analyzer angle of nanowire–polymer fiber (red) and nanocube–polymer fiber (blue) demonstrating significant polarized emission (P_{max} = 0.44) in the nanowire composite parallel to the fiber axis, as compared to the nanocube composite (P_{max} = 0.08).

polarized light (P = 0.36) compared to no polarization for $CsPbBr_3$ nanocubes.[33]

We assign the polarized emission from the perovskite–nanowire to its very anisotropic shape and the fact that the wavelength of the exciting light (480 nm) is much greater than the wire diameter (10 nm). This results in a dielectric confinement effect: When the incident field is polarized parallel to the wire, the electric field inside the wire is not reduced since it is mainly affected by the micrometer-long wire's dielectric constant. However, when polarized perpendicular to the wire (10 nm diameter), the electric field amplitude is attenuated due to the effective dielectric constant of the combined perovskite–polymer medium.[38]

LONG-TERM RETENTION OF QUANTUM YIELD UPON WATER-SOAKING OF PEROVSKITE–POLYMER COMPOSITES

To investigate the resistance of the nanocomposites to water, photoluminescence quantum yield measurements were conducted using an integrating sphere photoluminescence spectrograph. Measurements on ~150 μm thick nanocube–SEBS films immersed continuously in water were conducted periodically for 122 days. The sample's absolute photoluminescence quantum yield is unchanged over that period (Figures 4 and S2). Similar results are observed in much thinner 1.5 μm thick

DOI: 10.1021/acsami.6b09443
ACS Appl. Mater. Interfaces 2016, 8, 35523–35533

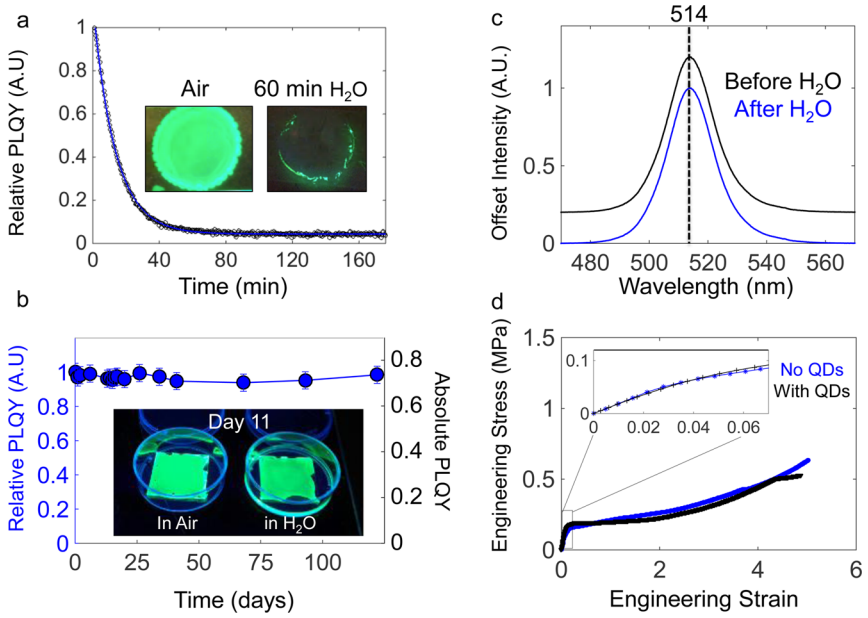

Figure 4. (a) Relative quantum yield of as-synthesized nanocubes in water as a function of soaking time in mins (black). The quantum yield decay is fitted to a monoexponential function (blue), where the decay coefficient is 16 min, demonstrating the as-synthesized QDs' sensitivity to water. The perovskite QD degradation is visible to the naked eye, as shown in pictures of drop-casted as-synthesized samples, excited with UV (λ = 365 nm) before and after 60 min of water soaking. (b) Relative and absolute quantum yield of 150 μm thick nanocubes−polymer composite films after >4 months of water-soaking, indicating retention of high quantum yield. Thin 3 μm spun-cast composite films also demonstrate enhanced water stability as illustrated by (Inset pictures) after 11 days of soaking in water and in air. (c) Composite emission spectra before and after 1 month of water soaking, indicating no changes to the spectra from the original 514 nm and fwhm of 17 nm. (d) No significant changes in the polymer's macroscopic mechanical properties is seen after QD incorporation, as demonstrated by tensile engineering stress−strain curves. Inset indicates first 0.07 strain.

composite films, as shown in Figure 4b. As-synthesized perovskite QDs completely lose their fluorescence after ∼60 min of contact with water (Figure 4a). Their luminescence quantum yields diminish exponentially, with a time constant of 16 min, due to the highly ionic nature and the large solubility-product constant of $PbBr_2$, which is orders of magnitude greater than other heavy metal compounds.[7] We extended our results on water stability to a second QD geometry, namely, strongly quantum-confined nanoplates. The nanoplates are more sensitive to structural changes, and emission shifts as a measure of water-induced QD degradation, e.g., loss of quantum confinement, are easier to detect. An important criterion in determining the stability of the composite is the photoluminescence emission spectrum, i.e., its shape, peak maximum, and line width. Figure 4c illustrates that there was no change in the emission spectra before and after 60 days of water immersion, consistent with little to no damage to the polymer-encapsulated nanocubes and nanoplates (see Figure S3).

This result far exceeds that seen in previous work for any perovskite material, including perovskite thin films coated with polymer films.[15,17,18,22] The enhanced water stability is assigned to the perovskite QDs' surface passivation, which consists of long alkyl ligand chains that are chemically compatible with the hydrophobic polymer, forming a strong polymeric−ligand interface that ultimately prevents access of water to the QD surface.[17,18,23] We postulate that due to their ionic nature ligand-free perovskites form weaker interfaces with nonpolar-hydrophobic polymers, which causes their previously reported poor stability upon exposure to water.[17,18,22]

Due to their different compositions, there are differences in stability and water/oxygen diffusion between the three polymers. First, the contact angle that water makes with each polymer, as measured by contact angle measurements, is different. The contact angle is ∼87 for polystyrene,[40] ∼100 for SEBS[41] and ∼110 for PLMA.[42] Since higher angles mean lower wettability, the wettability follows the trend of PS > SEBS > PLMA. Qualitatively, SEBS and PS polymers provide water stability for long durations, whereas quantitatively we monitored water stability for perovskite−SEBS composites which showed no change in PLQY for more than 100 days on end. SEBS was used for PLQY measurements due to its high flexibility, which makes the sample preparation easier. Regarding oxygen diffusion, SEBS adopts a microphase separated structure,[43] with domains ∼25 nm in size. Any entering oxygen will encounter both PS and EB blocks after only several dozen nanometers.[43] The EB block of the SEBS triblock copolymer has higher oxygen diffusion than the PS block, since oxygen is impeded by the aromatic groups in PS.[44] However, since the SEBS polymer we are using is 60% PS, it likely has similar oxygen diffusion to pure PS. Unlike SEBS and PS, PLMA is a viscous liquid that flows readily at room temperature[45] and thus has higher water and oxygen diffusion rates due to its high chain mobility. Accordingly, we found that PLMA−nanocrystal composites, while qualitatively stable for weeks in air, exhibited partial solubility in water. After a week of immersion in water, the polymer film visibly decreased in size due to being dissolved into water; thus, this polymer was not suited for long-term water stability assessments. We found that stability properties are more dependent on the type of the polymer host matrix rather than the type of perovskite nanocrystal, i.e., in SEBS and PS polymer, we have observed that all nanocrystal−polymer composites can survive without any apparent harm or PLQY reduction for long duration in water. We note that recent work shows that similar polymeric encapsulation can also improve the onset of thermal

DOI: 10.1021/acsami.6b09443
ACS Appl. Mater. Interfaces 2016, 8, 35523−35533

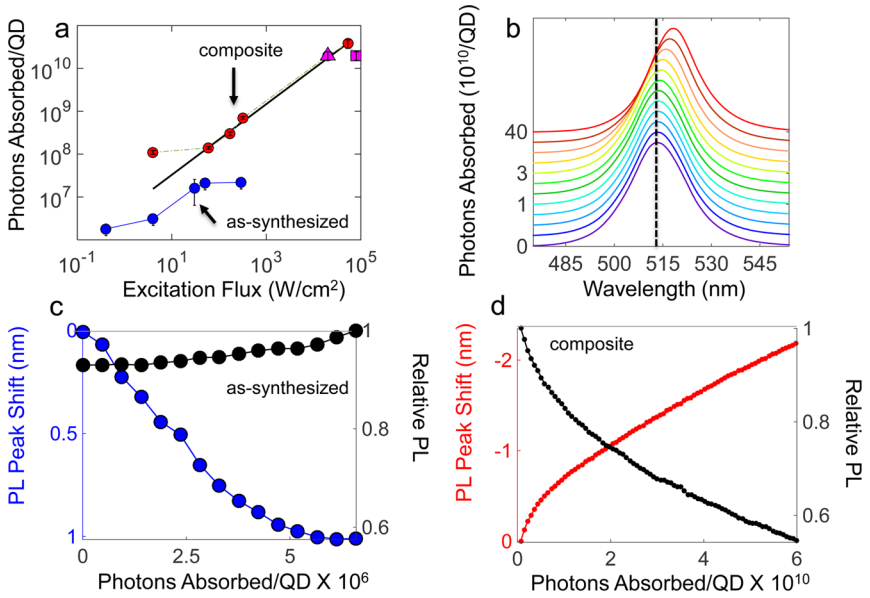

Figure 5. Enhanced light stability in perovskite−polymer composites. (a) Measurements of photons absorbed per quantum dot prior to photodegradation as a function of excitation flux. Comparing as-synthesized QDs (blue) and composites (SEBS red) (PS magenta) shows a clear enhancement in the composites. A power−law-like model (exponent value of 0.83) fits the high fluxes but deviates at low fluxes suggesting a diffusion-controlled degradation pathway. (b) Selection of normalized raw emission spectra of nanocube−polymer composite as a function of number of photons absorbed per quantum dot, demonstrating the typical degradation pathway of the composites. Spectra are arbitrarily offset for clarity; dashed line is a guide to the eye. (c) Representative light-soaking trial of as-synthesized QDs film at a flux of 30 W/cm^2, illustrating photobrightening (black) and initial blueshifts (blue) indicative of photodegradation. (d) Representative light-soaking trial of nanocube−polymer composite at a flux of 5.3×10^4 W/cm^2 as a function of number of photons absorbed per quantum dot, suggesting a different degradation pathway, with observed photobleaching (black) and red-shifting (red) at high fluxes.

degradation of the perovskite nanocrystals from ∼85 C in air to ∼110 C via encapsulation in PS.[25]

We also tested the quasi-static tensile and dynamic mechanical properties of the composites.[46,34,47] Figure 4d shows a typical tensile mechanical curve to failure before and after incorporation of the nanocubes into the polymer. Specifically, films with optical density 0.1 were made using a nanocube concentration of 1.5 μmol (∼0.5% by weight) in the polymer. The mechanical properties of the block copolymer were maintained with a toughness (defined as the area under the stress−strain curve) of ∼1.5 MPa, Young's modulus ∼2 MPa, and ductility >400% before and after nanocube incorporation. These mechanical properties were maintained even after prolonged (60 days) exposure to water. We also assessed the tan delta, or ratio of loss modulus to storage modulus, of the films as a function of strain. We find that this property is generally maintained after nanoparticle addition, which implies that low concentrations (∼5% by weight) of QD incorporation do not significantly degrade the viscoelastic behavior of the polymer (Figure S4).[48]

Lead toxicity raises concerns for the use of perovskites in many situations. To determine if lead escaped from the nanocube−polymer composites (SEBS, optical density 0.1, thickness ∼150 μm) over a period of 90 days of water-soaking, inductively coupled atomic emission spectroscopy (ICP-AES) was conducted. Lead concentration in water which the polymer was soaked in was comparable (∼20 parts per billion) to its concentration in tap water (within experimental error) and was 200 times higher for the same concentration of unencapsulated, as-synthesized QDs, dissolved in the same volume of water (Figure S5). From ICP-MS data (Figure S5) one can estimated water penetration depth of ∼50 nm into the ∼100 μm thick polymer nanocomposite. The low water penetration depth (only 0.05% of the total polymer composite layer thickness) could explain the result of minimum decrease in PLQY over the course of more than 100 days. This demonstrates that the polymers not only protect the perovskite QDs from the environment but also effectively protect the environment from the toxic lead.

SUBSTANTIALLY ENHANCED PHOTOSTABILITY IN PEROVSKITE-POLYMER COMPOSITES

All three shapes of colloidal perovskite QDs in this work are highly luminescent and promising candidates for future downshifting photoluminescence technologies, where high photostability under constant illumination is critical. The photon budget, i.e., the number of photons absorbed before spectral shifting and photobleaching, is a crucial figure of merit for QD-based devices.[29,30] We performed light-soaking experiments on perovskite−polymer composites in order to determine their photon budget and compared them with as-synthesized nanocubes. The experiment was conducted both in PS and SEBS polymers and over 5 orders of magnitude of fluxes, ranging from 0.3 to 5×10^4 W/cm^2. Only composites with low optical density (∼0.05−0.1) were used for light-soaking experiments, an optical density range similar to those in QD based displays.[49] We quantified our results using the arbitrary metric of number of photons absorbed per QD prior to 1 nm of spectral peak shift (a spectral red-shift in the composites and blue-shift for as-synthesized nanocubes)[30,50] (see Supporting Information Methods, Tables S1−S2, and Figures S6−S7). In Figure 5c,d, we show typical results where we compare spectra from as synthesized QDs and the composites. As-synthesized QDs undergo blue-shifting (blue line) and photobrightening (∼5−10% black line). These changes are typical signatures of photo-oxidation and chemical

DOI: 10.1021/acsami.6b09443
ACS Appl. Mater. Interfaces 2016, 8, 35523−35533

degradation that lead to shrinkage of the QDs size and passivation of long-lived surface defect states.[51,52] After further illumination, these blue-shifts were followed by red-shifts and more photobrightening (~20%), which implies sintering of the individual QDs (see Figure S7). Indeed, at the highest excitation flux of 5×10^4 W/cm^2, as-synthesized samples decomposed with clearly visible damage within 1−2 s of laser illumination (Figure S8). Very different trends were observed for the composites. Initially, no significant change was seen in the spectral shape of the emission, indicating light-soaking-stability of most QDs (Figure 5b). Finally, for QD−SEBS composites, degradation is manifested in a distinct red-shift with no photobrightening or blue-shifting, indicating that the polymer is protecting the QDs from photoinduced degradation pathways, probably by blocking ambient oxygen from reaching the QD surface. As a result the composites survive high fluxes of 5×10^4 W/cm^2, orders of magnitude higher than unprotected cubes. While both samples have eventual spectral red-shifts, the number of photons absorbed per QD in the PS and SEBS composite is up to 4 orders of magnitude higher than that of the as-synthesized QDs (Figures S6 and S7). The perovskite−polymer composites demonstrated high photostability of $>10^{10}$ absorption events, while as-synthesized nanocubes reached only $\sim 10^6-10^7$ before spectral-shifting (Figures 5a, S6, and S7). For comparison, a typical semiconductor QD photon budget is $\sim 10^8-10^9$ photons absorbed prior to photodegradation.[30,50,52] This metric was assessed in previous work via the number of photons absorbed to complete photobleaching of single QDs, a metric which does not consider spectral shifts; however, even slight spectral shifts of 1−2 nm are important for optical downshifting applications. Because previous metrics did not consider spectral shifts, they provide a higher estimate than the metric in this work. It is important to note that studies on light stability have not been reported for the latest generation of near-unity quantum yield CdSe dots, which may be more stable.

The mechanism of the red-shift during light exposures in this work is likely to be induced aggregation through heating effects because of phonon generation during nonradiative recombination in the quantum dot composites, similar to the work of Wang et al.[53] Another possibility is that the red-shifting is due to degradation of the blue (smaller) quantum dot population. Smaller crystals have a higher surface to volume ratio. Small, blue emitting quantum dots will die faster than bigger red emitting ones due to harmful photo-oxidation processes; thus, the total emission could redshift. This is usually also accompanied by decrease in the emission fwhm, which was not observed here.

Figure 5a demonstrates the number of photons absorbed before spectral shifting as a function of excitation flux. The data exhibits a power-law-like distribution. At low fluxes, the deviation from this trend is assigned to the kinetics of the degradation mechanism. The photoinduced degradation is a diffusion-controlled reaction, which is limited by the rate of O_2 diffusion through the polymeric matrix. From our data, we estimate a reaction rate constant of $k = 10^8$ M^{-1} s^{-1} for the photodegradation. This rate is an order of magnitude slower than the literature limit for diffusion-controlled reactions in solvents. This is a reasonable value since the SEBS and PS polymer matrices are significantly more impermeable to O_2 diffusion and viscous than standard solvents, which also limits the ability of the QDs to diffuse.[27,54] This slow photo-oxidation rate gives rise to the record-high photon budget that we demonstrate, which to the best of our knowledge is the highest photon budget reported in the literature to date for any quantum dot or dye fluorophores.[29,30] The protection that perovskite−polymer composites provide is of relevance for down-shifting devices such as backlit displays.

As mentioned above, the range of concentrations used in this work is reasonably relevant to actual real-world display applications, which have typical optical densities for green-emitting quantum dots of ~0.04.[55] We have been able to vary the optical density in the range of 0.01−1 by changing the amount of moles of nanocrystal cubes added to the solution prior to drop-casting or spin-coating the polymer films. We have not found the nanocrystal concentration in the polymer to affect water stability much. Both high (OD $\geq$ 0.75) and low (OD $\approx$ 0.05−0.75) concentrations in SEBS polymer were stable in the water for long time periods. In contrast, light stability tests are concentration sensitive; higher optical densities (0.75−1) experienced local heating effects which quickly degrade the sample. However, these concentrations are higher than those typically used in applications.[49,55]

CONCLUSION

We have demonstrated advantages properties for perovskite QD−polymer composites. By changing the shape of the nanocrystalline component and mechanically aligning anisotropic nanocrystals in polymer fibers, emergent properties such as polarization and color tunability can be achieved. Although perovskite QDs are sensitive to light and water, their stability markedly increases through macroscale polymer encapsulation. The composites demonstrated high photoluminescence quantum yield after months of soaking in water and survive up to $>10^{10}$ photons absorbed per QD before significant spectral shifts. The light stability and retention of quantum yield upon water exposure seen in this work is likely due to the comparatively strong interface formed between the native hydrophobic surface coating on the perovskite QDs and the hydrophobic polymers. A similar perovskite ligand−hydrophobic polymer matching scheme may also benefit bulk and thin film perovskites. Finally, in light of the encouraging ability of these composites to prevent toxic lead leakage, they have potential for real-world optical device applications, such as optically pumped lasers and polarized downshifters.

MATERIALS AND METHODS

Materials. All chemicals were used as received from their respective sources: poly(styrene-ethylene-butylene-styrene) (SEBS, MD-1537), ~120 kDa, Kraton corporation; poly(lauryl methacrylate) solution (PLMA, 30% by weight in toluene, Aldrich); polystyrene (PS 187 kDa, Aldrich); Cs_2CO_3 (99.9%, Aldrich); octadecene (ODE, 90%, Aldrich); oleic acid (OA, 90%, Aldrich); $PbBr_2$ (99.999%, Aldrich); oleylamine (OLA, 70%, Aldrich); octylamine (OCT, 99%, Aldrich); hexane (99.9%, Fisher Scientific); toluene (99.9%, Aldrich).

Nanocrystal Synthesis. Nanocubes, nanoplates, and nanowires were prepared as described previously.[9−11]

Preparation of Cesium Oleate. Both 0.4 g of Cs_2CO_3 and 1.2 mL of OA were loaded into a 3-necked flask along with 15 mL of ODE, degassed under vacuum at 120 °C for 1 h, following a second degassing phase at 150 °C under Ar until all Cs_2CO_3 reacted with OA.

Synthesis of $CsPbBr_3$ QDs. ODE (5 mL) and $PbBr_2$ (0.069g, 99.999%, Aldrich) were loaded into a 25 mL 3-necked flask and

DOI: 10.1021/acsami.6b09443
ACS Appl. Mater. Interfaces 2016, 8, 35523−35533

dried under vacuum for 1 h at 120 °C. Dried oleylamine (0.5 mL, OLA, 70%, Aldrich) and dried OA (0.5 mL) were injected at 120 °C under Ar. After complete solubilization of a $PbBr_2$ salt, the injection temperature was set, and hot (~100 °C) cesium oleate solution (0.4 mL, 0.125 M in ODE, prepared as described above) was quickly injected. The reaction mixture was immediately cooled by the ice−water bath. Injection temperatures of 150−180 °C produce nanocubes, while temperatures of 90−130 °C produce nanoplates. For nanowires, 0.8 mL of dried OCT, and 0.8 mL of dried OLA were injected at 120 °C successively, instead of the above amounts.

Preparation of Polymer−Nanocrystal Composite Films and Fibers. After centrifugation from the reaction solution, all shapes of nanocrystals (NCs, NPLs, and NWs) were cleaned twice using hexane as solvent and ethyl acetate or methyl-ethyl-ketone as nonsolvent since typical alcohol or acetone washing techniques degrade the nanocrystals. Next, nanocrystals were dispersed in toluene (note that the polymers employed in this work only dissolve in toluene but not hexane.)

In particular, as-made perovskite nanowires may lose their PL even under these mild cleaning conditions; this is assigned to the long synthetic process which depletes the surface ligand coverage. We have developed a surface treatment with the native ligand and $PbBr_2$ precursors that enables us to reconstruct the surface and protective ligand layer which ultimately restores with the high PLQY values.

For the surface treatment, anhydrous toluene (5 mL), $PbBr_2$ (0.188 mmol, X = Cl or Br), OA (0.5 mL), and OLA (0.65 mL) were added to a scintillation vial all within an argon inert atmosphere glovebox. The solution was stirred at 100 °C within the glovebox until the complete dissolution of the $PbBr_2$ salt occurs; this may take several hours. The resulting concentrated stock solution is stable at room temperature but is stored in a glovebox to maintain dryness of the solution over time. A cleaned wire solution was then mixed with the above solution and stirred at 85 °C until the solution turned turbid. The NWs were isolated by centrifugation at 6000 rpm for 5 min and redispersed in toluene for further use. The surface treatment dramatically increases the PLQY and morphological stability of as-synthesized wires.

Nanocomposites were then formed by mixing nanocrystal and polymers in toluene (30, 30, and 20% by weight, for PLMA, SEBS, and PS, respectively). After mixing and sonicating to form uniform dispersions, the solutions were cast onto glass slides (SEBS) and dried overnight. Thin films were spin-coated onto coverslips (PLMA and PS, 500 or 1000 rpm for 30 s) or wound into fiber arrays (PLMA). To draw the fibers, ~30 μL of a PLMA solution in toluene (30% by weight) was added to a nanocrystal solution in a volume of toluene of ~30 μL in a 1 mL disposable glass vial. This highly viscous mixture was vortexed and sonicated for 60 min to ensure uniform mixing and deposited onto a glass slide. After 2 min, needles or tweezers were used to draw fibers straight from the deposit onto any substrate.

The moles of nanoparticles added to the three polymers for all nanocrystal shapes varied from about 0.5−15 μM for optical densities of 0.05−1 respectively. The volume of spin-cast or drop-cast as-synthesized nanocubes was typically around 10 μL. For 1.5−3 μm thick polystyrene films with optical density ~0.05−0.1, the volume of solution used was typically around ~10 μL. For ~100 μm thick polymer films, ~ 200 μL of solution was cast onto a glass slide. The above quantities used were consistent for all three nanocrystal shapes. For all nanocrystal shapes, low optical density composites had optical densities of 0.05−0.1, while the high optical density composites ranged from 0.75 to 1.

For the cubes, the concentration that was later on applied for the estimation of photon absorption per nanoparticle was determined by using previously published extinction coefficient.[27] By measuring transmittance intensity attenuation with an optical microscope. (We have taken extra care and verified that scattering and reflectance from these samples are negligible.) We use the film thickness as assessed by atomic force microscopy for films ≤3 μm thick or digital calipers with an accuracy of ~1 μm for films ~100 μm in thickness. We use the Gaussian laser beam radius to obtain the effective illuminated volume and determine the number of quantum dots we excite.

For obtaining the molar concentration of NPLs and NWs, we multiplied the previously reported wavelength-dependent intrinsic absorption coefficient at the excitation wavelength used by the respective nanocrystal volume. This resulted in extinction coefficients of 1.4×10^6 and 0.014×10^6 cm^{-1} for NWs and NPLs, respectively.

Characterization of Absorbance (Optical Density). Polymer films were characterized using an Agilent 8453 UV−visible spectroscopy system. Optical density values are reported for the 488 nm wavelength.

Monitoring of Photoluminescence Quantum Yield (PLQY). PLQY was monitored using a lab-built integrating sphere spectrofluorometer, as described in detail previously.[35] Briefly, the sample was placed in a cylindrical glass cuvette (FireflySci, 75UV) with a PTFE cap and was excited with 488 nm light from a Fianium SC450 supercontinuum laser at a power density of ~36 W/mm^2. The laser spot size was roughly 1 mm. The composite samples were cut into 30 × 8 mm strips and fitted into the cuvette. The emitted light from the sample exits the integrating sphere through a 6.4 mm exit port and passed through an SP2300 monochromator before being detected with a thermoelectrically cooled silicon CCD camera (PIXIS 400B). The laser power was measured continually using a ThorLabs S120VC silicon photodiode.

For determining the absolute value of the PLQY, we used a reference sample of pure toluene or hexane (no nanocrystals) for perovskite nanocrystals in toluene or hexane, while for polymer films, a reference sample of a pure polymer film of the same dimensions and thickness (no nanocrystals) was utilized. For nanocrystal−polymer films in water, a pure polymer film (no nanocrystals) of the same dimensions and thickness immersed in water was utilized.

Transmission Electron Microscopy (TEM). Transmission electron micrographs were acquired using a Tecnai G220 S-TWIN TEM equipped with a Gatan SC200 CCD camera. Images were acquired using an accelerating voltage of 200 kV. Image-J was used for analyzing nanoparticle size distributions.

Measurements of Film Thickness. The thickness of the films was measured with a digital micrometer (Mitutoyo, 293−831−30, resolution 1 um) and an atomic force microscope (Veeco Multimode).

Quasi-Static Tensile Mechanical Testing and Continuous Dynamic Analysis. Mechanical tests on SEBS films were performed using an Agilent T-150 nanomechanical tensile tester.[34,47] In dynamic mechanical analysis, small oscillatory forces are used to monitor the evolution of the viscoelastic properties of the polymer as a function of strain.[34] The value of tan delta represents a convolution of the loss factor (which

DOI: 10.1021/acsami.6b09443
ACS Appl. Mater. Interfaces 2016, 8, 35523−35533

increases with increased viscous behavior) and storage modulus (which increases with increased elastic behavior) and thus is a measure of how the overall viscoelastic properties change during application of a tensile stress. Testing was performed as described previously.[34] The strain rate was set to 10^{-2} for SEBS films, which were mounted into the tensile tester using standard pivot grips. The harmonic force amplitude was 4.5 mN, while the oscillation frequency was 20 Hz.[47]

Inductively Coupled Plasma Atomic Emission Spectrometry (ICP-AES). The lead concentration of water that was in contact with nanocubes−SEBS composites (optical density 0.1) for 90 days was determined by using an Optima 7000 DV ICP-AES (PerkinElmer). Serial dilutions of a lead standard solution in 2% nitric acid (Sigma-Aldrich) were prepared spanning a wide range as calibration solutions. Nanocube samples were prepared for comparison by drying under nitrogen followed by dissolving with nitric acid and dilution to a 10 mL volume with water. The water that the perovskite nanocomposites was soaked in was diluted to a volume of 10 mL, and 2% by weight nitric acid was added. All samples contained 2% by weight of nitric acid.

Measurement of Emission Polarization from Polymer Nanocomposite Fibers. The nanowire-PLMA composites were excited with a 488 nm Ar+ laser (Lexel Laser, Inc., 95). Extra care was taken to achieve circular polarization of the excitation laser. Bright-field and fluorescence images were taken with a digital microscope camera (Paxcam 2+), as seen in Figure 3. The polarization fluorescence of the nanocrystals was monitored using a Zeiss inverted fluorescence microscope with a spectrometer (Acton Research Corporation, SpectraPro-3001) and CCD detector (Princeton Instruments, Model 7509−0001). Varying exposure times of 0.5−1 s were used to collect spectra. To analyze the emitted light polarization, we used a rotation mounted linear polarizer in the emission path.

■ ASSOCIATED CONTENT

Supporting Information

The Supporting Information is available free of charge on the ACS Publications website at DOI: 10.1021/acsami.6b09443.

Absorption, photoluminescence, and mechanical data, pictures of films, and additional information (PDF)

■ AUTHOR INFORMATION

Corresponding Author

*E-mail: paul.alivisatos@berkeley.edu.

ORCID

Shilpa N. Raja: 0000-0001-5641-8930

Matthew A. Koc: 0000-0003-1401-8415

Robert O. Ritchie: 0000-0002-0501-6998

Author Contributions

S.N.R. and Y.B. contributed equally to this work.

Notes

The authors declare no competing financial interest.

■ ACKNOWLEDGMENTS

This work is supported by the Physical Chemistry of Inorganic Nanostructures Program, KC3103 (for Y.B., P.Y., and A.P.A) and by the Inorganic/Organic Nanocomposites Nanoscale Science, Engineering, and Technology Program (for S.N.R., M.A.K., and R.O.R.), Office of Basic Energy Sciences of the U.S. Department of Energy, under contract number DE-AC02-05CH11231 for both programs. D.Z. is grateful for fellowship support from Suzhou Industrial Park. S.F. acknowledges scholarship support from the German Research Foundation (DFG, agreement FI 2042/1-1). L.L. was supported by National Science Foundation NSF Grant ECCS-0901864 for mechanical characterization support. We thank Noah Bronstein, Steven Hawks, Wojciech Osowiecki, and Matthew Jones for helpful discussions and Elena Kreimer, Nicholas J. Borys, Andrew Wong, Natalie Gibson, Samuel Eaton, Zeke Liu, Brent Koscher, and Joseph Swabeck for experimental assistance.

■ REFERENCES

(1) Lee, M. M.; Teuscher, J.; Miyasaka, T.; Murakami, T. N.; Snaith, H. J. Efficient Hybrid Solar Cells Based on Meso-Superstructured Organometal Halide Perovskites. *Science* **2012**, *338*, 643−647.

(2) Im, J.-H.; Lee, C.-R.; Lee, J.-W.; Park, S.-W.; Park, N.-G. 6.5% Efficient Perovskite Quantum-Dot-Sensitized Solar Cell. *Nanoscale* **2011**, *3*, 4088−4093.

(3) McMeekin, D. P.; Sadoughi, G.; Rehman, W.; Eperon, G. E.; Saliba, M.; Horantner, M. T.; Haghighirad, A.; Sakai, N.; Korte, L.; Rech, B.; Johnston, M. B.; Herz, L. M.; Snaith, H. J. A Mixed-Cation Lead Mixed-Halide Perovskite Absorber for Tandem Solar Cells. *Science* **2016**, *351*, 151−155.

(4) Wang, H.-C.; Lin, S.-Y.; Tang, A.-C.; Singh, B. P.; Tong, H.-C.; Chen, C.-Y.; Lee, Y.-C.; Tsai, T.-L.; Liu, R.-S. Mesoporous Silica Particles Integrated with All-Inorganic CsPbBr3 Perovskite Quantum-Dot Nanocomposites (MP-PQDs) with High Stability and Wide Color Gamut Used for Backlight Display. *Angew. Chem., Int. Ed.* **2016**, *55*, 7924−7929.

(5) Dou, L.; Yang, Y. M.; You, J.; Hong, Z.; Chang, W.-H.; Li, G.; Yang, Y. Solution-Processed Hybrid Perovskite Photodetectors with High Detectivity. *Nat. Commun.* **2014**, *5*, 5404.

(6) Wei, H.; Fang, Y.; Mulligan, P.; Chuirazzi, W.; Fang, H.-H.; Wang, C.; Ecker, B. R.; Gao, Y.; Loi, M. A.; Cao, L.; Huang, J. Sensitive X-Ray Detectors Made of Methylammonium Lead Tribromide Perovskite Single Crystals. *Nat. Photonics* **2016**, *10*, 333−339.

(7) Hailegnaw, B.; Kirmayer, S.; Edri, E.; Hodes, G.; Cahen, D. Rain on Methylammonium Lead Iodide Based Perovskites: Possible Environmental Effects of Perovskite Solar Cells. *J. Phys. Chem. Lett.* **2015**, *6*, 1543−1547.

(8) Grätzel, M. The Light and Shade of Perovskite Solar Cells. *Nat. Mater.* **2014**, *13*, 838−842.

(9) Protesescu, L.; Yakunin, S.; Bodnarchuk, M. I.; Krieg, F.; Caputo, R.; Hendon, C. H.; Yang, R. X.; Walsh, A.; Kovalenko, M. V. Nanocrystals of Cesium Lead Halide Perovskites (CsPbX 3, X = Cl, Br, and I): Novel Optoelectronic Materials Showing Bright Emission with Wide Color Gamut. *Nano Lett.* **2015**, *15*, 3692−3696.

(10) Bekenstein, Y.; Koscher, B. A.; Eaton, S. W.; Yang, P.; Alivisatos, A. P. Highly Luminescent Colloidal Nanoplates of Perovskite Cesium Lead Halide and Their Oriented Assemblies. *J. Am. Chem. Soc.* **2015**, *137*, 16008−16011.

(11) Zhang, D.; Eaton, S. W.; Yu, Y.; Dou, L.; Yang, P. Solution-Phase Synthesis of Cesium Lead Halide Perovskite Nanowires. *J. Am. Chem. Soc.* **2015**, *137*, 9230−9233.

(12) Yakunin, S.; Protesescu, L.; Krieg, F.; Bodnarchuk, M. I.; Nedelcu, G.; Humer, M.; De Luca, G.; Fiebig, M.; Heiss, W.; Kovalenko, M. V. Low-Threshold Amplified Spontaneous Emission and Lasing From Colloidal Nanocrystals of Caesium Lead Halide Perovskites. *Nat. Commun.* **2015**, *6*, 8056.

(13) Pan, J.; Sarmah, S. P.; Murali, B.; Dursun, I.; Peng, W.; Parida, M. R.; Liu, J.; Sinatra, L.; Alyami, N.; Zhao, C.; Alarousu, E.; Ng, T. K.; Ooi, B. S.; Bakr, O. M.; Mohammed, O. F. Air-Stable Surface-Passivated Perovskite Quantum Dots for Ultra-Robust, Single- and Two-Photon-Induced Amplified Spontaneous Emission. *J. Phys. Chem. Lett.* **2015**, *6*, 5027−5033.

(14) Quan, L. N.; Yuan, M.; Comin, R.; Voznyy, O.; Beauregard, E. M.; Hoogland, S.; Buin, A.; Kirmani, A. R.; Zhao, K.; Amassian, A.;

Kim, D. H.; Sargent, E. H. Ligand-Stabilized Reduced-Dimensionality Perovskites. *J. Am. Chem. Soc.* **2016**, *138*, 2649−2655.
(15) Palazon, F.; Akkerman, Q. A.; Prato, M.; Manna, L. X-Ray Lithography on Perovskite Nanocrystals Films: From Patterning with Anion-Exchange Reactions to Enhanced Stability in Air and Water. *ACS Nano* **2016**, *10*, 1224−1230.
(16) Kulbak, M.; Cahen, D.; Hodes, G. How Important Is the Organic Part of Lead Halide Perovskite Photovoltaic Cells? Efficient CsPbBr3 Cells. *J. Phys. Chem. Lett.* **2015**, *6*, 2452−2456.
(17) Habisreutinger, S. N.; Leijtens, T.; Eperon, G. E.; Stranks, S. D.; Nicholas, R. J.; Snaith, H. J. Carbon Nanotube/Polymer Composites as a Highly Stable Hole Collection Layer in Perovskite Solar Cells. *Nano Lett.* **2014**, *14*, 5561−5568.
(18) Leijtens, T.; Eperon, G. E.; Noel, N. K.; Habisreutinger, S. N.; Petrozza, A.; Snaith, H. J. Stability of Metal Halide Perovskite Solar Cells. *Adv. Energy Mater.* **2015**, *5*, 1500963.
(19) Kinjo, N.; Ogata, M.; Nishi, K.; Kaneda, A.; Dušek, K. *Speciality Polymers/Polymer Physics*; Springer-Verlag, Berlin, 1989; p 3.
(20) Dubertret, B.; Skourides, P.; Norris, D. J.; Noireaux, V.; Brivanlou, A. H.; Libchaber, A. In Vivo Imaging of Quantum Dots Encapsulated in Phospholipid Micelles. *Science* **2002**, *298*, 1759−1762.
(21) Huang, H.; Chen, B.; Wang, Z.; Hung, T. F.; Susha, A. S.; Zhong, H.; Rogach, A. L. Water Resistant CsPbX3 Nanocrystals Coated with Polyhedral Oligomeric Silsesquioxane and Their Use as Solid State Luminophores in All-Perovskite White Light-Emitting Devices. *Chem. Sci.* **2016**, *7*, 5699−5703.
(22) Hwang, I.; Jeong, I.; Lee, J.; Ko, M. J.; Yong, K. Enhancing Stability of Perovskite Solar Cells to Moisture by the Facile Hydrophobic Passivation. *ACS Appl. Mater. Interfaces* **2015**, *7*, 17330−17336.
(23) Bockstaller, M.; Mickiewicz, R.; Thomas, E. Block Copolymer Nanocomposites: Perspectives for Tailored Functional Materials. *Adv. Mater.* **2005**, *17*, 1331−1349.
(24) Pathak, S.; Sakai, N.; Wisnivesky Rocca Rivarola, F.; Stranks, S. D.; Liu, J.; Eperon, G. E.; Ducati, C.; Wojciechowski, K.; Griffiths, J. T.; Haghighirad, A. A.; Pellaroque, A.; Friend, R. H.; Snaith, H. J. Perovskite Crystals for Tunable White Light Emission. *Chem. Mater.* **2015**, *27*, 8066−8075.
(25) Wang, Y.; He, J.; Chen, H.; Chen, J.; Zhu, R.; Ma, P.; Towers, A.; Lin, Y.; Gesquiere, A. J.; Wu, S.-T.; Dong, Y. Ultrastable, Highly Luminescent Organic-Inorganic Perovskite-Polymer Composite Films. *Adv. Mater.* **2016**, DOI: 10.1002/adma.201603964.
(26) Pan, J.; Quan, L. N.; Zhao, Y.; Peng, W.; Murali, B.; Sarmah, S. P.; Yuan, M.; Sinatra, L.; Alyami, N. M.; Liu, J.; Yassitepe, E.; Yang, Z.; Voznyy, O.; Comin, R.; Hedhili, M. N.; Mohammed, O. F.; Lu, Z. H.; Kim, D. H.; Sargent, E. H.; Bakr, O. M. Highly Efficient Perovskite-Quantum-Dot Light-Emitting Diodes by Surface Engineering. *Adv. Mater.* **2016**, *28*, 8718−8725.
(27) De Roo, J.; Ibáñez, M.; Geiregat, P.; Nedelcu, G.; Walravens, W.; Maes, J.; Martins, J. C.; Van Driessche, I.; Kovalenko, M. V.; Hens, Z. Highly Dynamic Ligand Binding and Light Absorption Coefficient of Cesium Lead Bromide Perovskite Nanocrystals. *ACS Nano* **2016**, *10*, 2071−2081.
(28) Raja, S. N.; Olson, A. C. K.; Limaye, A.; Thorkelsson, K.; Luong, A.; Lin, L.; Ritchie, R. O.; Xu, T.; Alivisatos, A. P. Influence of Three-Dimensional Nanoparticle Branching on the Young's Modulus of Nanocomposites: Effect of Interface Orientation. *Proc. Natl. Acad. Sci. U. S. A.* **2015**, *112*, 6533−6538.
(29) Wang, C.; Bai, C. *Single Molecule Chemistry and Physics*; Springer Science & Business Media: New York, 2006; p 507.
(30) Kuno, M.; Fromm, D. P.; Hamann, H. F.; Gallagher, A.; Nesbitt, D. J. On"/ "Off" Fluorescence Intermittency of Single Semiconductor Quantum Dots. *J. Chem. Phys.* **2001**, *115*, 1028−1040.
(31) Meyns, M.; Perálvarez, M.; Heuer-Jungemann, A.; Hertog, W.; Ibáñez, M.; Nafria, R.; Genç, A.; Arbiol, J.; Kovalenko, M. V.; Carreras, J.; Cabot, A.; Kanaras, A. G. Polymer-Enhanced Stability of Inorganic Perovskite Nanocrystals and Their Application in Color Conversion LEDs. *ACS Appl. Mater. Interfaces* **2016**, *8*, 19579−19586.
(32) Babin, V.; Fabeni, P.; Nikl, M.; Pazzi, G. P.; Sildos, I.; Zazubovich, N.; Zazubovich, S. Polarized Luminescence of CsPbBr3 Nanocrystals (Quantum Dots) in CsBr:Pb Single Crystal. *Chem. Phys. Lett.* **1999**, *314*, 31−36.
(33) Wang, D.; Wu, D.; Dong, D.; Chen, W.; Hao, J.; Qin, J.; Xu, B.; Wang, K.; Sun, X. Polarized Emission From CsPbX3 Perovskite Quantum Dots. *Nanoscale* **2016**, *8*, 11565−11570.
(34) Raja, S. N.; Basu, S.; Limaye, A. M.; Anderson, T. J.; Hyland, C. M.; Lin, L.; Alivisatos, A. P.; Ritchie, R. O. Strain-Dependent Dynamic Mechanical Properties of Kevlar to Failure: Structural Correlations and Comparisons to Other Polymers. *Mater. Today Commun.* **2015**, *2*, e33−e37.
(35) Bronstein, N. D.; Yao, Y.; Xu, L.; O'Brien, E.; Powers, A. S.; Ferry, V. E.; Alivisatos, A. P.; Nuzzo, R. G. Quantum Dot Luminescent Concentrator Cavity Exhibiting 30-Fold Concentration. *ACS Photonics* **2015**, *2*, 1576−1583.
(36) Powers, A. S.; Liao, H.-G.; Raja, S. N.; Bronstein, N. D.; Alivisatos, A. P.; Zheng, H. Tracking Nanoparticle Diffusion and Interaction During Self-Assembly in a Liquid Cell. *Nano Lett.* **2016**, DOI: 10.1021/acs.nanolett.6b02972.
(37) Chen, F.; Gerion, D. Fluorescent CdSe/ZnS Nanocrystal-Peptide Conjugates for Long-Term, Nontoxic Imaging and Nuclear Targeting in Living Cells. *Nano Lett.* **2004**, *4*, 1827−1832.
(38) Wang, J.; Gudiksen, M. S.; Duan, X.; Cui, Y.; Lieber, C. M. Highly Polarized Photoluminescence and Photodetection From Single Indium Phosphide Nanowires. *Science* **2001**, *293*, 1455−1457.
(39) Hu, J.; Li, L. S.; Yang, W.; Manna, L.; Wang, L. W.; Alivisatos, A. P. Linearly Polarized Emission from Colloidal Semiconductor Quantum Rods. *Science* **2001**, *292*, 2060−2063.
(40) Li, Y.; Pham, J. Q.; Johnston, K. P.; Green, P. F. Contact Angle of Water on Polystyrene Thin Films: Effects of CO2 Environment and Film Thickness. *Langmuir* **2007**, *23*, 9785−9793.
(41) Ramaratnam, K.; Tsyalkovsky, V.; Klep, V.; Luzinov, I. Ultrahydrophobic Textile Surface via Decorating Fibers with Monolayer of Reactive Nanoparticles and Non-Fluorinated Polymer. *Chem. Commun.* **2007**, *43*, 4510−4512.
(42) Chanda, J.; Ionov, L.; Kirillova, A.; Synytska, A. New Insight Into Icing and De-Icing Properties of Hydrophobic and Hydrophilic Structured Surfaces Based on Core−Shell Particles. *Soft Matter* **2015**, *11*, 9126−9134.
(43) Raja, S. N.; Zherebetskyy, D.; Wu, S.; Ercius, P.; Powers, A.; Olson, A. C. K.; Du, D. X.; Lin, L.; Govindjee, S.; Wang, L.-W.; Xu, T.; Alivisatos, A. P.; Ritchie, R. O. Mechanisms of Local Stress Sensing in Multifunctional Polymer Films Using Fluorescent Tetrapod Nanocrystals. *Nano Lett.* **2016**, *16*, 5060−5067.
(44) Chen, J.; Huang, X.; Jiang, P.; Wang, G. Protection of SEBS/PS Blends Against Gamma Radiation by Aromatic Compounds. *J. Appl. Polym. Sci.* **2009**, *112*, 1076−1081.
(45) Sadoway, D. R. Block and Graft Copolymer Electrolytes for High-Performance, Solid-State, Lithium Batteries. *J. Power Sources* **2004**, *129*, 1−3.
(46) Raja, S. N.; Luong, A. J.; Zhang, W.; Lin, L.; Ritchie, R. O.; Alivisatos, A. P. Cavitation-Induced Stiffness Reductions in Quantum Dot−Polymer Nanocomposites. *Chem. Mater.* **2016**, *28*, 2540−2549.
(47) Basu, S.; Hay, J. L.; Swindeman, J. E.; Oliver, W. C. Continuous Dynamic Analysis: Evolution of Elastic Properties with Strain. *MRS Commun.* **2014**, *4*, 25−29.
(48) Raja, S. N.; Olson, A. C. K.; Thorkelsson, K.; Luong, A. J.; Hsueh, L.; Chang, G.; Gludovatz, B.; Lin, L.; Xu, T.; Ritchie, R. O.; Alivisatos, A. P. Tetrapod Nanocrystals as Fluorescent Stress Probes of Electrospun Nanocomposites. *Nano Lett.* **2013**, *13*, 3915−3922.
(49) Kubista, M.; Sjöback, R.; Eriksson, S.; Albinsson, B. Experimental Correction for the Inner-Filter Effect in Fluorescence Spectra. *Analyst (Cambridge, U. K.)* **1994**, *119*, 417−419.
(50) Boisseau, P.; Lahmani, M. *Nanoscience: Nanobiotechnology and Nanobiology*; Springer Science & Business Media: Berlin, 2010; p 149.
(51) Park, Y.-S.; Guo, S.; Makarov, N. S.; Klimov, V. I. Room Temperature Single-Photon Emission From Individual Perovskite Quantum Dots. *ACS Nano* **2015**, *9*, 10386−10393.

(52) van Sark, W. G. J. H. M.; Frederix, P. L. T. M.; Van den Heuvel, D. J.; Gerritsen, H. C.; Bol, A. A.; van Lingen, J. N. J.; de Mello Donegá, C.; Meijerink, A. Photooxidation and Photobleaching of Single CdSe/ZnS Quantum Dots Probed by Room-Temperature Time-Resolved Spectroscopy. *J. Phys. Chem. B* **2001**, *105*, 8281−8284.
(53) Wang, Y.; Li, X.; Sreejith, S.; Cao, F.; Wang, Z.; Stuparu, M. C.; Zeng, H.; Sun, H. Photon Driven Transformation of Cesium Lead Halide Perovskites From Few-Monolayer Nanoplatelets to Bulk Phase. *Adv. Mater.* **2016**, DOI: 10.1002/adma.201604110.
(54) Atkins, P.; de Paula, J. *Physical Chemistry*; Macmillan: New York, 2006; p 879.
(55) Jang, E.; Jun, S.; Jang, H.; Lim, J.; Kim, B.; Kim, Y. White-Light-Emitting Diodes with Quantum Dot Color Converters for Display Backlights. *Adv. Mater.* **2010**, *22* (28), 3076−3080.

DOI: 10.1021/acsami.6b09443
ACS Appl. Mater. Interfaces 2016, 8, 35523−35533